Preprints, Sixth Conference on Mesoscale Processes, Portland, OR, AMS, July, 18-22, 1994, pp. 619-622.

6.06 MULTICELL SQUALL LINE STRUCTURE AS A MANIFESTATION OF VERTICALLY TRAPPED GRAVITY WAVES

Ming-Jen Yang and Robert A. Houze, Jr.

Department of Atmospheric Sciences
University of Washington, AK-40
Seattle, Washington 98195

1. INTRODUCTION

A multicell thunderstorm often consists of a series of evolving convective cells at any given time. Convective cells typically form on or near the storm periphery at 10 to 15 min intervals. Each cell within the storm goes through a similar life cycle and each eventually becomes the dominant cell of the storm complex, building to higher levels as it approaches and finally merges with the main storm complex (Browning 1977). Precipitation forms in the new updraft and is held aloft temporarily while the cell intensifies. Finally precipitation unloads as the cell matures, resulting in a heavy gush of rain. At low levels, cooler air diverging from the downdrafts encounters the incoming warmer air along a gust front, creating a region of strong convergence favorable for development of new convective cells. The result is a series of new cells that tend to form along the gust front.

Often multicell thunderstorms are found in a squall line, which is a long-lived line of laterally aligned cells that tend not to interfere disruptively with one another by competing for the same warm, moist environmental air. A vertical cross section taken perpendicular to the squall line often shows a series of convective cells at different stages of their evolution.

The objective of this study is to consider the multicellular structure of a midlatitude squall line from the viewpoint of gravity-wave dynamics. The squall line to be investigated in this study is the 10-11 June 1985 squall line during the PRE-STORM project (Cunning 1986).

2. NUMERICAL MODEL

The numerical model used in this study is a two-dimensional version of the Klemp and Wilhelmson (1978) compressible cloud model, as modified by Wilhelmson and Chen (1982). The bulk microphysical parameterization used in the model is of the type described by Lin et al. (1983) with some improvements suggested by Potter (1991). The basic-state environment is assumed constant in time and horizontally homogeneous. Large-scale motion, Coriolis force, surface drag, and radiation effects are neglected. Stretched grids are used in both vertical and horizontal directions (similar to Fovell and Ogura 1988). The grid size of the lowest layer is 140 m; the grid size of the highest layer is 550 m; and the model top is at 21.7 km. A 315-km wide fine mesh with 1-km resolution is in the center of the domain; 2,250-km wide stretched grids are on both sides of the fine mesh.

The initial thermodynamic and wind profiles for the simulation are identical to those used by Yang and Houze (1992), and are characterized by a CAPE of 3,323 J kg^{-1}, and a bulk Richardson number of 46.9. A 5-km deep, 170-km long cold pool with maximum strength of –6 °K was placed in the domain to initiate convection.

3. SIMULATION RESULTS

After t = 8 h, the simulated squall line reaches its mature stage. Figure 1 is the time sequence of surface rainfall rate during an one-hour period (t =10–11 h) in the mature stage. It shows the continuous generation of intense precipitation cells at the leading edge and much weaker precipitation in the trailing stratiform region. In the instantaneous model outputs at t = 11 h (Figs. 2 and 3), convective-scale features are evident. The vertical velocity with a shaded precipitation field (defined as radar reflectivity > 5 dBZ) in Fig. 2 exhibits the typical structure of a multicell storm, i.e., a sequence of convective cells at different stages of their evolution. However, when the vertical velocity field is superimposed on other field, a new interpretation of the multicellular structure can be obtained—*convective cells in a multicell storm are associated with gravity waves.*

In Fig. 3, minima of p' (defined as the deviations from the initial value) are located one quarter of a wavelength behind (to the left of) the updrafts in lower troposphere (z < 3.5 km), but the minima p' are located one quarter of a wavelength ahead (to the right) of the updrafts in upper troposphere (7 km <z < 13 km). This phase relationship can be seen clearly for the updraft located at x = 13 to 23 km. Although the heights of updraft centers for the convective cells (Fig. 2) are different, their phase

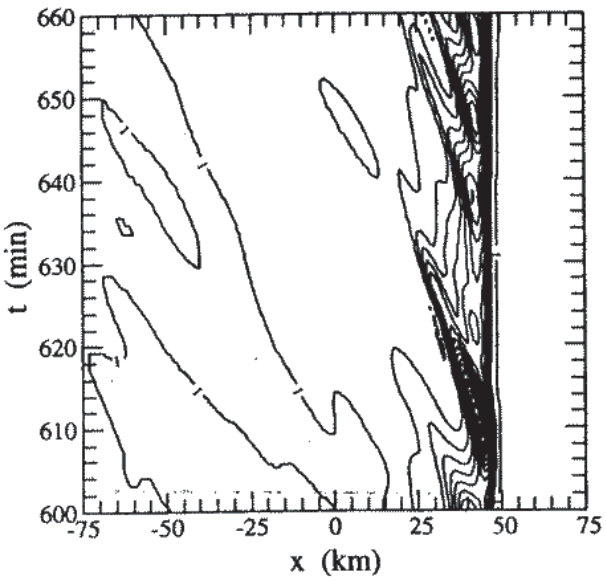

Fig. 1 Time history of surface rainfall rate during an one-hour period (600-660 min). Contour lines start from 1 mm h^{-1} with an interval of 10 mm h^{-1}. It is displayed in a storm-relative coordinate moving at a speed of 12 m s^{-1} relative to the ground.

relationships with p' fields (Fig. 3) are the same. The distinct phase relationships between the w and p' fields in the troposphere indicate that the multicellular structure is indeed a gravity wave phenomenon.

Disturbances above the tropopause (z > 14 km) in Figs. 2 and 3 show a structure typical of vertically propagating gravity waves (cf. Fig. 4.1 of Durran 1990). The gravity waves above the tropopause are mechanically triggered by convective cells constantly impinging upon the tropopause (Fovell et al. 1992).

In Figure 2, the low-level convective updraft at the gust front (x = 50 km) is a persistent feature of the simulated mature-phase squall line. Convective cells behind the low-level leading-edge cell, on the other hand, are transient wave features. These "gravity-wave" updrafts form by breaking away from the top of the low-level gust-front updraft. Once the gravity-wave updrafts are separated from the persistent gust-front updraft, they propagate rearward at their associated gravity-wave phase speeds. The regeneration period of gravity-wave updrafts is 11–17 min, which is the same as the generation period of precipitation cells in the surface rainfall rate field (Fig. 1).

The convective-cell trajectories in Fig. 4a are determined by tracking the motion of updraft centers from model output at 2-min intervals during the one-hour period between t = 10–11 h. The imaginary convective-cell trajectories determined from surrounding airflows are in Fig. 4b, starting from the same points as the trajectories in Fig. 4a. All trajectories are displayed in a storm-relative coordinate where the gust front is fixed at x = 50 km. Comparison of the trajectories in Fig. 4a and Fig. 4b shows that *the updraft cells move at velocities significantly different from the airflows in their near surroundings*. Behind the gust front (x <50 km in Fig. 4), the convective updraft cells always propagate rearward relative to the gust front, regardless of the direction of the airflows in their near environments. Therefore, updraft cells that break away from the top of the low-level gust-front updraft move at the phase speeds of their associated gravity waves, not at mean airflow speeds as implied by the traditional multicell model (Browning 1977; Weisman and Klemp 1986). The rearward propagation of convective cells within the storm is due to the westward (front-to-rear) phase speeds of their associated gravity waves. The multicellular storm structure thus arises because the propagation speed of the density current associated with the cold pool differs from the phase speed of the gravity waves it generates.

4. LINEAR THEORY

In this section, we use linear gravity-wave theory to explain the multicellular structure seen in the nonlinear numerical simulation. Following Durran (1989), the anelastic linear governing equations for a two-dimensional internal gravity wave in a nonrotating flow in which a basic state only varies with height are

$$\left(\frac{\partial}{\partial t}+\overline{U}\frac{\partial}{\partial x}\right)u'+w'\frac{d\overline{U}}{dz}=-c_p\overline{\theta}\frac{\partial \pi'}{\partial x} \qquad (1)$$

$$\left(\frac{\partial}{\partial t}+\overline{U}\frac{\partial}{\partial x}\right)w'=-c_p\overline{\theta}\frac{\partial \pi'}{\partial z}+g\frac{\theta'}{\overline{\theta}} \qquad (2)$$

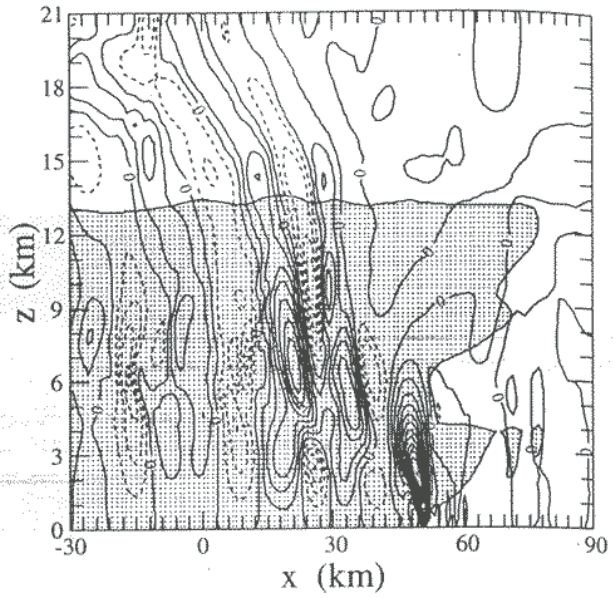

Fig. 2 Vertical velocity (with a contour interval of 1 m s^{-1}) of the simulated storm at t = 11 h. The positive field is in solid lines and the negative field is dashed. Radar reflectivity greater than 5 dBZ is shaded. The leading edge of gust front is at x = 50 km.

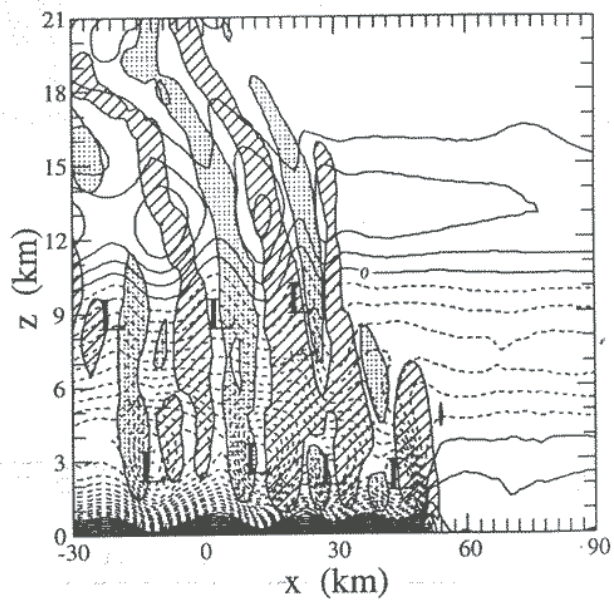

Fig. 3 Pressure perturbation (with a contour interval of 0.3 mb) of the simulated storm at t = 11 h. The positive field is in solid lines and the negative field is dashed. Vertical velocity greater than 1 m s^{-1} is hatched, and vertical velocity less than -1 m s^{-1} is shaded. The detailed vertical velocity structure can be seen in Fig. 2. A letter L denotes a region of low pressure.

$$\left(\frac{\partial}{\partial t}+\overline{U}\frac{\partial}{\partial x}\right)\theta'+\frac{\overline{\theta}}{g}N^2w'=Q \tag{3}$$

$$\frac{\partial}{\partial x}(\overline{\rho}u')+\frac{\partial}{\partial z}(\overline{\rho}w')=0 \tag{4}$$

Variables in (1) –(4) are in their traditional symbols; zonal wind u, vertical velocity w, nondimensional pressure π, potential temperature θ, buoyancy frequency N, and Q is the latent-heating produced by convection. The basic-state variables $\overline{\rho}, \overline{U}, \overline{\theta}$, and $\overline{\pi}$ are functions of height; perturbations are defined by primes; $u = \overline{U} + u'$, $w = w'$, $\pi = \overline{\pi} + \pi'$, $\theta = \overline{\theta} + \theta'$.

After some algebraic manipulation of (1)–(4), we can obtain a single equation for w, which is similar to equation (4.28) of Durran (1990) for the discussion of mountain waves. Since the basic-state variables are functions of height, we can assume solution of w of this form,

$$w=\left(\frac{\rho_o}{\overline{\rho}}\right)^{1/2}\mathrm{Re}\left\{W(z)e^{ik(x-ct)}\right\}$$

$$Q=\frac{\overline{\theta}}{g}\left(\frac{\rho_o}{\overline{\rho}}\right)^{1/2}\mathrm{Re}\left\{H(z)e^{ik(x-ct)}\right\} \tag{5}$$

where ρ_o is the reference density (surface density), Re means the real part of a complex variable, k is the wavenumber, and c is the phase speed. In (5), we assume that latent heating is horizontally in phase with vertical velocity, which is generally true for deep convection. Substitution of (5) into the governing equation leads to

$$\frac{d^2W}{dz^2}+(\ell^2-k^2)W=\frac{H}{(\overline{U}-c)^2} \tag{6}$$

where

$$\ell^2\approx\frac{N^2}{(\overline{U}-c)^2} \tag{7}$$

ℓ^2 is called the Scorer parameter (Scorer 1949). The lower boundary condition for (6) is a rigid lid, and the upper boundary condition is a "radiation condition," that allows energy to propagate upward through the top of the domain (Lindzen 1974). The Scorer parameter in Fig. 5 is determined from the horizontally averaged profiles of $\overline{U}$ and N for a 70-km-wide region of the leading portion of the squall line at time t = 11 h (x = –20 to 50 km in Figs. 2 and 3). Ground-relative phase speed is c = –20 m s^{-1} is determined from a time-lapse display of model results with a data resolution of 2 min. For the region of x = –10 to 26 km in Figs. 2 and 3, k is –2π/(16 km). The latent-heating profile H is determined from numerical model output at t = 11 h for that region. For given k, c, $\overline{U}$, N, and H we can use the method of Lindzen and Kuo (1969) to solve equation (6) for W numerically. Once w is solved, u', π', and θ' can be determined from (1)–(4).

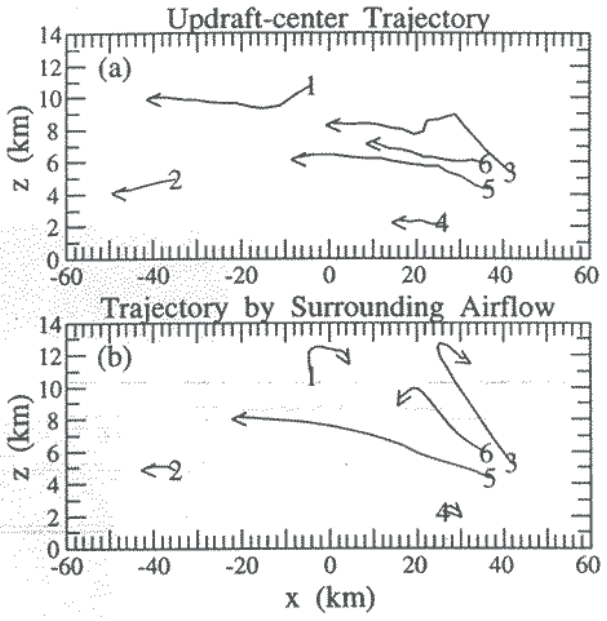

Fig. 4 (a) Updraft-center trajectories and (b) the imaginary updraft-cell trajectories determined from the surrounding airflows during the time period t = 10–11 h. The arrowhead at the end point of each trajectory indicates its direction.

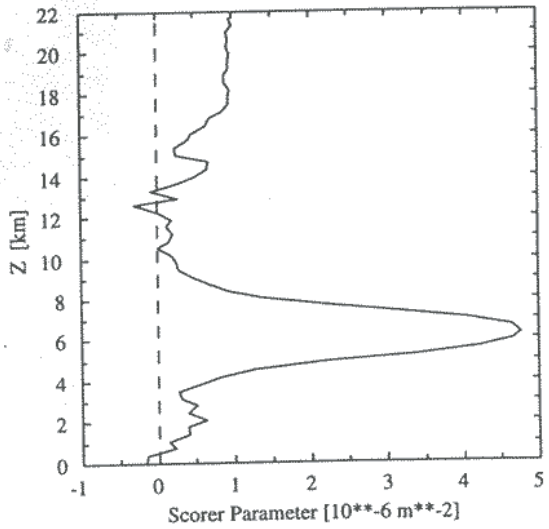

Fig. 5 Scorer parameter ℓ^2 averaged horizontally over a 70-km wide region (x = –20 to 50 km) for the simulated storm at t = 11 h.

5. DISCUSSION

Fig. 6a shows the w and p' perturbation fields predicted by the linear theory for the region of x = 10–26 km at time t = 11 h, and Fig. 6b is the corresponding numerical model result. Linear theory predicts the right strength (7.9 m s^{-1}) of the updraft at the right level (~7.3 km), when compared with nonlinear numerical model output. Linear theory also captures the strong vertical tilt of the phase line in the lower stratosphere. Linear theory shows that p' minima are

to the left of the updrafts in lower troposphere and to the right of the updrafts in upper troposphere, which are also seen in the nonlinear numerical model result. Thus the phase relationship between the p' and w fields is well predicted by linear theory. These results demonstrate that the multicellular structure is basically controlled by linear gravity-wave dynamics.

In the leading portion of the simulated squall line, the dominant horizontal wavelengths are $\lambda = 16$ to 20 km, and storm-relative phase speeds are $c = -20$ to -25 m s^{-1}, so the main gravity-wave periods in this region are $T = \lambda/c$ =10.7-16.7 min, which are the same as the generation periods of precipitation cells (11–17 min) at the mature stage (see Fig. 1). In the trailing stratiform region, the gravity waves become more diffuse with weaker amplitudes, and their wavelengths become larger ($\lambda = 25$–35 km) with increasing phase speeds (storm-relative phase speeds are c = –30 to –40 m s^{-1}). According to the dispersion relation of two-dimensional internal gravity waves (equation 7.44 of Holton 1992), the increase of phase speed with increasing horizontal wavelength is a characteristic of the dispersion of internal gravity waves. The opposite phase relationships of w and p' fields between the lower and upper troposphere, moreover, indicate that these gravity waves are vertically trapped within the troposphere.

According to equation (6), for a given k, the vertical profile of the Scorer Parameter determines whether waves will be trapped or propagating in the vertical. The reason for the waves to be trapped in the mid-to-upper levels (6 km < z< 13 km) is the strong decrease of Scorer parameter with height (Fig. 5), as in the case of trapped lee waves (Durran 1990). Recalling the definition of the Scorer parameter in (7), the strong decrease of Scorer parameter with height in mid-to-upper levels of the storm results from both an increase of wind speed $\overline{U}$ and a decrease of static stability N with height (not shown). These features of the shear and instability are associated with the internal storm structure.

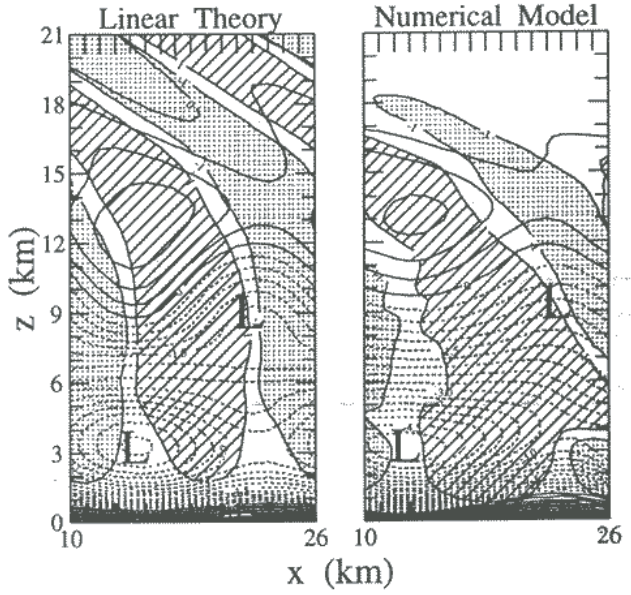

Fig. 6 (a) As in Fig. 3 except for those predicted by the linear theory and (b) determined from the numerical model for x = 10–26 km at t = 11 h.

That is, the rear inflow at midlevels and front-to-rear flow above constitute an environment favorable for trapping of waves triggered at the gust front. Waves are also trapped in low levels (0 < z < 6 km) because of the destructive interference with waves reflected from the ground.

Acknowledgement: This research was supported by National Science Foundation Grant ATM-9101653.

REFERENCES

Browning, K. A., 1977: The structure and mechanisms of hailstorms. *Hail: A Review of Hail Science and Hail Suppression* (G. B. Foote and C. A. Knight, Eds.), American Meteorological Society, Boston, 1–43.

Cunning, J. B., 1986: The Oklahoma-Kansas Preliminary Regional Experiment for STORM-Central. *Bull. Amer. Meteor. Soc.*, **67**, 1478–1486.

Durran, D. R., 1989: Improving the anelastic approximation. *J. Atmos. Sci.*, **46**, 1453–1461.

———, 1990: Mountain waves and downslope winds. *Atmospheric Processes over Complex Terrain* (W. Blumen, Ed.), American Meteorological Society, Boston, 59–81.

Fovell, R. G., and Y. Ogura, 1988: Numerical simulation of a midlatitude squall line in two dimensions. *J. Atmos. Sci.*, **45**, 3846–3879.

———, D. Durran, and J. R. Holton, 1992: Numerical simulations of convectively generated stratospheric gravity waves. *J. Atmos. Sci.*, **49**, 1427–1442.

Holton, J. R., 1992: *An Introduction to Dynamic Meteorology*, Academic Press, 3rd ed, 507 pp.

Klemp, J. B., and R. B. Wilhelmson, 1978: The simulation of three-dimensional convective storm dynamics. *J. Atmos. Sci.*, **35**, 1070–1096.

Lin, Y. L., R. D. Farley, and H. D. Orville, 1983: Bulk parameterization of the snow field in a cloud model. *J. Climate Appl. Meteor.*, **22**, 1066–1092.

Lindzen, R. S., 1974: Wave-CISK in the tropics. *J. Atmos. Sci.*, **31**, 156–179.

———, and H.-L. Kuo, 1969: A reliable method for the numerical integration of a large class of ordinary and partial differential equations. *Mon. Wea. Rev.*, **97**, 732–734.

Potter, B. E., 1991: Improvement to a commonly used cloud microphysical bulk parameterization. *J. Appl. Meteor.*, **30**, 1040-1042.

Scorer, R. S., 1949: Theory of waves in the lee of mountains. *Quart. J. Roy. Meteor. Soc.*, **75**, 41–56.

Weisman, M. L., and J. B. Klemp, 1982: The dependence of numerically simulated convective storms on wind shear and buoyancy. *Mon. Wea. Rev.*, **110**, 504–520.

———, and ———, 1986: Characteristics of convective storms. *Mesoscale Meteorology and Forecasting* (P. S. Ray, Ed.), American Meteorological Society, Boston, 331–358.

Wilhelmson, R. B., and C.-S. Chen, 1982: A simulation of the development of successive cells along a cold outflow boundary. *J. Atmos. Sci.*, **39**, 1466–1483.

Yang, M.-J., and R. A. Houze, Jr., 1992: A numerical study of the momentum budget of a squall line. *Preprints, 11th International Conf. on Clouds and Precipitation*, Montreal, Canada, Amer. Meteor. Soc., 719-722.